ADVANCED FUNCTIONAL MATERIALS
www.afm-journal.de

A LiF Nanoparticle-Modified Graphene Electrode for High-Power and High-Energy Lithium Ion Batteries

Zhong-Shuai Wu, Lili Xue, Wencai Ren, Feng Li, Lei Wen, and Hui-Ming Cheng**

Surface modification of carbon materials plays an important role in tailoring carbon surface chemistry to specify their electrochemical performance. Here, a surface modification strategy for graphene is proposed to produce LiF-nanoparticle-modified graphene as a high-rate, large-capacity pre-lithiated electrode for high-power and high-energy lithium ion batteries. The LiF nanoparticles covering the active sites of the graphene surface provide an extra Li source and act as an effective solid electrolyte interphase (SEI) inhibiter to suppress $LiFP_6$ electrolyte decomposition reactions, affect SEI components, and reduce their thickness. Consequently, the Li-ion diffusion is greatly sped up and the thermodynamic stability of the electrode is significantly improved. This modified graphene electrode shows excellent rate capability and improved first-cycle coulombic efficiency, cycling stability, and ultrahigh power and energy densities accessible during fast charge/discharge processes.

1. Introduction

High-power lithium ion batteries (LIBs) are becoming increasingly important for powering transportation systems, such as hybrid electric vehicles (HEVs), plug-in HEVs, and electric vehicles.[1–9] Graphene as a novel two-dimensional carbon is expected to be a high-rate electrode candidate for high-power LIBs because of its unique advantages in energy storage.[10–24] Among the developed strategies, chemical exfoliation/reduction of graphite oxide is a more practical low-cost way to produce graphene on a large scale.[25–28] The as-prepared graphene can meet the quantity requirement for LIB applications and, for example, has been widely used to improve the rate capability and cycling stability of traditional electrode materials like oxides.[11–13,16,19,21–24] Chemically-derived graphene is different in that it consists not only of sp^2 hybridized carbon but also contains oxygen and hydrogen heteroatoms which are present as active functional groups such as hydroxyl, carboxyl, carboxylic, and lactone on the plane and edges of graphene layers.[29] Due to its rich surface chemistry, surface side reactions at the interface between the electrode and electrolyte must be considered, in particular, a solid electrolyte interphase (SEI) film will be formed, which seriously influences the electrochemical behavior of graphene.[30–32]

The SEI film is formed by a surface-related process, and it is inhomogeneous, electronically insulating and composed of both inorganic and organic components.[30–35] Normally, a thin, stable and compact film of inorganic products (such as LiF, Li_2O, Li_2CO_3) as protection function is located on the surface of the electrode, while a thicker, possibly porous film of organic products (polymeric and oligomeric), that is permeable to the electrolyte, is formed on the electrolyte side and acts as a transport medium for lithium ions.[30,31] Previous studies reported that the morphology and structure (thickness, component, and size) of the SEI films could be optimized and their passivation could be minimized by surface modification of carbon electrodes.[35] The dispersion of metallic nanoparticles of Sn, Al, Pt, Ag,[36] and the use of electrolyte additives[37,38] (e.g., dimethyl pyrocarbonate,[39] alkyl-sulfite,[40,41] phosphate,[42] vinylene carbonate,[43,44] tris(pentafluorophenyl) borane,[45] tetrachloroethylene,[46] SO_2,[47] CO_2),[48] etc. were developed to tailor carbon surface chemistry and improve their electrochemical performance, including lowering surface impedance, suppressing gas evolution, improving thermal stability, increasing electrical conductivity, lowering viscosity co-solvents, processing high charge/discharge capability, reducing first cycle irreversible capacity, extending cyclic life, and improving lower-temperature performance.[30,31,49] These studies proved the critical importance of surface modification for carbon electrode materials, in particular, appropriate surface passivation reactions on carbon electrodes, for improving their resulting Li-storage performance.[30,49]

Recently, our group demonstrated that the complex surface chemistry of graphene (atomic percentage of oxygen ~8.55%) can strongly induce SEI passivation by electrolyte reduction or decomposition on the electrolyte-wetted electrode surface, making it suffer from capacity fluctuation under fast charge and discharge.[32] This phenomenon is intrinsically attributed to the thermodynamic instability of the graphene electrode induced by the rapid electrolyte (such as $LiFP_6$) reduction with the oxygen-containing functional groups on graphene, resulting in the formation of an inhomogeneous SEI film.[32–35,50] Therefore, we believed that a sufficient homogeneous SEI formation on graphene by surface modification is important for improving the shelf life and safety of LIBs.

Dr. Z.-S. Wu, Dr. L. Xue, Dr. W. Ren, Dr. F. Li, Dr. L. Wen, Prof. H.-M. Cheng
Shenyang National Laboratory for Materials Science
Institute of Metal Research
Chinese Academy of Sciences
72 Wenhua Road, Shenyang 110016, P. R. China
E-mail: wcren@imr.ac.cn; cheng@imr.ac.cn

DOI: 10.1002/adfm.201200534

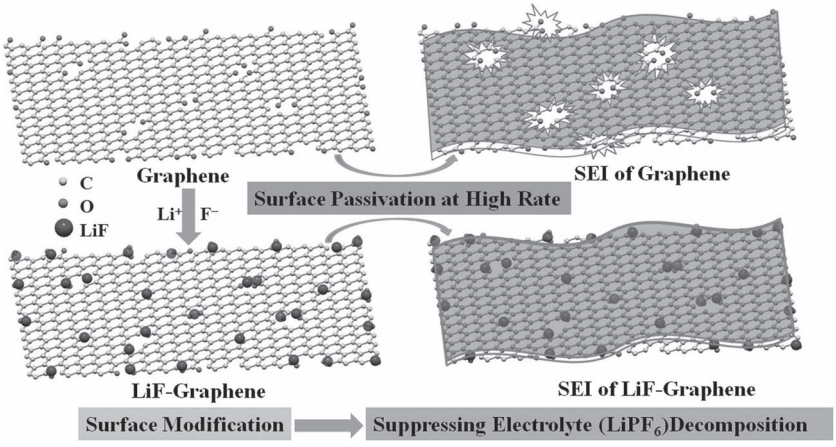

Scheme 1. Diagram of the formation of an ideal passivated SEI film at a high rate in the pristine graphene (top) and LiF nanoparticle-modified graphene (bottom) electrodes.

Herein we developed a surface modification strategy to produce LiF nanoparticle-modified graphene (LiF/graphene) as a pre-lithiated electrode material for high-power and high-energy LIBs. As shown in **Scheme 1**, LiF nanoparticles are anchored on the surface of graphene sheets, where they 1) cover active sites on the graphene surface as a $LiPF_6$ salt stabilizer and thus suppress the surface side reactions of $LiFP_6$ electrolyte decomposition and improve the interface stability, and provide an extra Li source; 2) directly become a component of the SEI film on the surface of graphene as a SEI forming inhibitor to reduce the thickness of the SEI layer; and 3) enhance the adhesion of the graphene surface to the SEI film, and consequently improve the thermodynamic stability and electrochemical performance of the graphene electrode. This graphene electrode, after LiF modification, is electrochemically-stable, and shows a large capacity at a rate of 0.82 C (~609 mAh g^{-1}) to 144 C (~181 mAh g^{-1}), high rate capability, and improved cyclability at fast charge and discharge processes. Significantly, the LiF/graphene electrode simultaneously achieves accessible ultrahigh power and energy densities (~30 kW $kg_{electrode}^{-1}$ & 238 Wh $kg_{electrode}^{-1}$) with a rate of tens of seconds (25 s), stressing the importance of the LiF addition for the surface modification of the graphene electrode in thermodynamic optimization of the SEI film between electrode and electrolyte.

2. Results and Discussion

2.1. Physicochemical Characterization

The morphology and structure of LiF/graphene were first investigated by scanning electron microscopy (SEM), transmission electron microscopy (TEM) and X-ray diffraction (XRD) techniques, as shown in **Figure 1**. It can be seen that LiF nanoparticles with a size of 5–15 nm are sparsely distributed on the surface of the graphene sheets (Figure 1a–d), and prevent their restacking (Figure 1b),[12,15] thus producing a flexible and electronically conductive framework with an open porous structure (Figure 1a). Due to the electrostatic interaction, it was speculated that the positively-charged Li^+ ions were primarily adsorbed on the negatively-charged oxygenated groups on the edges and defect sites (Figure 1c, Figure S1, Supporting Information).[12,15,51,52] High-resolution TEM (HRTEM) and fast Fourier transform (FFT) images reveal the good crystallinity of LiF nanoparticles with (002) plane on graphene (Figure 1e, Figure S2, Supporting Information), as confirmed by the XRD pattern (JCPDS 04-0857, Figure 1f) and X-ray photoelectron spectroscopy (XPS, Figure S3, Supporting Information). 11.6 wt% LiF on graphene was estimated from the XPS results. We should emphasize that the LiF nanoparticles strongly adhere to the graphene surface even after sonication during the preparation of TEM specimens.[12,15] This good adhesion is expected to improve the thermodynamic stability of both electrode and electrolyte.[30,31]

2.2. Electrochemical Characterization

Figure 2a shows the discharge (Li insertion)/charge (Li extraction) profiles of the LiF/graphene as a function of current rates from 0.5 A g^{-1} to 25 A g^{-1}. The modified graphene electrode exhibits negligible polarization and smooth charge/discharge profiles without capacity fluctuation,[32] and a higher first-cycle coulombic efficiency of 53% than does graphene (20–45%) at the same starting rate (Figure 2a), because of the extra Li source from LiF nanoparticles. It is suggested that the presence of LiF nanoparticles is beneficial to both the electrochemical stability of the electrolyte and its compatibility with graphene. At 0.5 A g^{-1} (0.82 C), the LiF/graphene can be fast charged to 609 mAh g^{-1} (Figure 2b,c). With increasing current rates, the LiF/graphene electrode shows a slight decrease in capacity. Significantly, it can be rapidly charged to a high capacity within several minutes to tens of seconds. For example, the capacity can be charged to 375 mAh g^{-1} at 2.5 A g^{-1} (6.7 C), 306 mAh g^{-1} at 5 A g^{-1} (16 C), and 242 mAh g^{-1} at 10 A g^{-1} (41 C). Even at a very high current rate of 25 A g^{-1} (144 C), although the charge time decreases about 150 times from 73 min to 25 s, the charge capacity (180 mAh g^{-1}) still remains as high as ~25.4% of the first reversible capacity (710 mAh g^{-1}) at 0.5 A g^{-1}. This result demonstrates the high rate capability of the LiF/graphene electrode for rapid charge-discharge processes, which is much better than that of other high-rate carbonaceous materials, such as graphite,[53] carbon monoliths,[54] nanotubes,[55] nanobeads,[56] and nanofibers.[57] Although the capacity of LiF/graphene at high rates, for example, at 25 A g^{-1}, is a little lower than those of B- or N-doped graphene (200–235 mAh g^{-1}),[32] the LiF/graphene shows a higher first reversible capacity than those of B- or N-doped graphene at 0.5 A g^{-1}. Besides the high rate capability, the LiF/graphene electrode also shows excellent cycling stability and good reversibility, as shown in Figure 2c. For example, the decrease in reversible capacity at high current densities of 2.5 ~ 25 A g^{-1} is smaller than 2.7% after 10 cycles for each rate. Furthermore, the reversible capacity can be

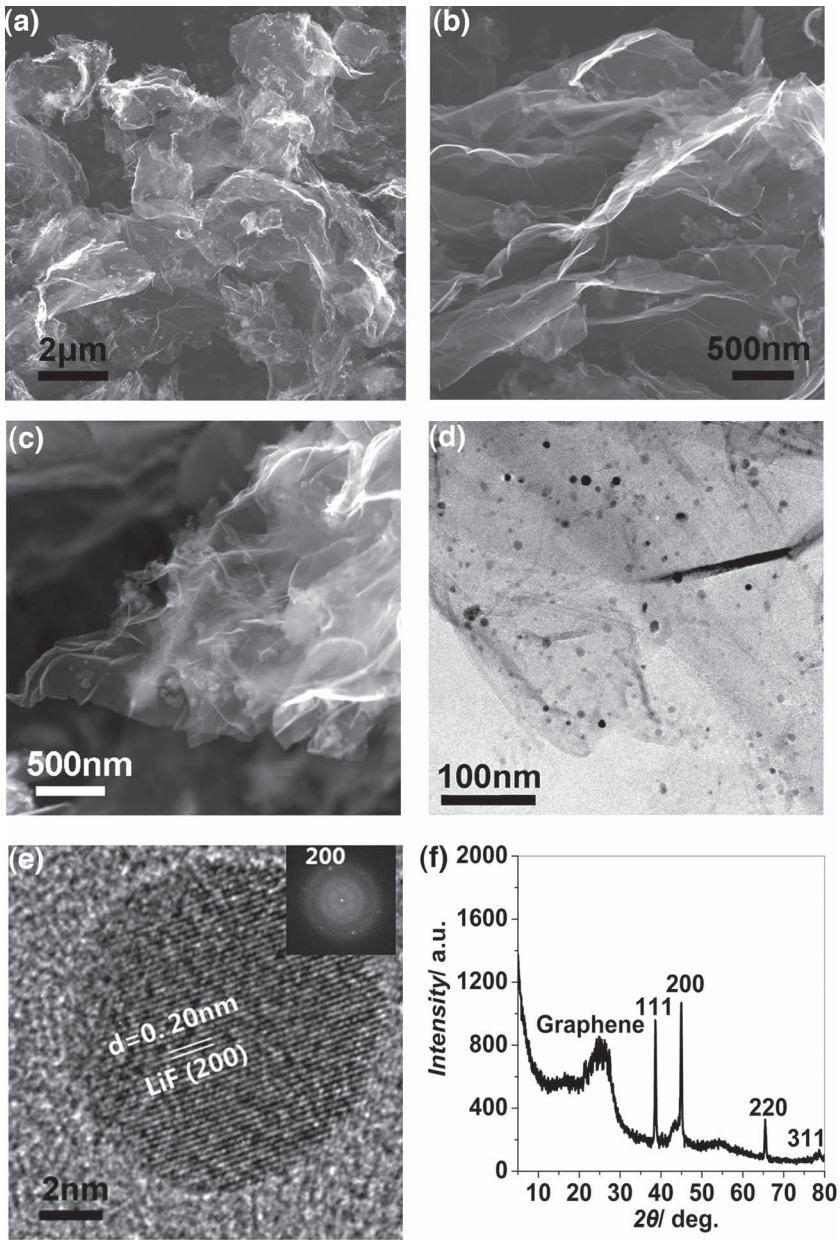

Figure 1. a) Low-magnification SEM image of the LiF/graphene. b) Side-view and c) edge-view high-magnification SEM images of the LiF/graphene. d) TEM image of the LiF/graphene. e) HRTEM image of a LiF nanoparticle anchored on the surface of graphene. Inset: reduced FFT image of the LiF nanoparticle. f) XRD pattern of the LiF/graphene.

recovered when the rate is reduced from 25 A g^{-1} to the initial 0.5 A g^{-1} after 80-cycles with different rates, and no significant capacity loss was observed during the following 70 cycles. A Ragone plot shows that the LiF/graphene has a very high power- and energy-density (Figure 2d). In particular, both the power (~30 kW $kg_{electrode}^{-1}$) and energy (238 Wh $kg_{electrode}^{-1}$) densities measured with a charge time of 25 s are significantly higher than those of graphene without LiF modification,[32] graphene oxide (GO),[32] thermally reduced GO at 500 °C (GO500) in H_2/Ar gas,[32] and are comparable to the power-oriented high-energy electrochemical supercapacitor electrodes of carbon nanotubes (~69.4 Wh $kg_{electrode}^{-1}$, or ~43.3 kW $kg_{electrode}^{-1}$)[58] and energy-oriented high-power LIB electrodes of $LiNi_{0.5}Mn_{0.5}O_2$,[2] $LiFePO_4$,[59] and $FePO_4$[60] alone at such a rate. All the above results demonstrate that the LiF/graphene is an excellent high-power and high-energy material.

2.3. SEI Film Characterizations

It is accepted that the electrode-electrolyte interaction determines the electrochemical performance of electrode materials for LIBs, and strongly depends on their surface chemistry.[61] In a well-defined electrolyte, the irreversible capacity of an electrode is mainly associated with the formation of the SEI film and other electrolyte decomposition products.[30,31] $LiFP_6$ is the most commonly used salt in electrolytes for LIBs because of its suitable dissociation constant in carbonate solvents, ionic mobility and electrochemical stability, and is usually dissolved in ethylene carbonate (EC) and dimethyl carbonate (DMC). However, $LiPF_6$ suffers from both hydrolytic and thermal instability.[45,62] The established dynamic equilibrium of the $LiPF_6$ salt with dissociated ions Li^+ and PF_6^- in the solvent is easily disturbed after its decomposition to form solid LiF and PF_5, and PF_5 readily hydrolyzes to form highly reactive HF and PF_3O on the electrode side.[38] As a consequence, the complex surface series reactions of the $LiFP_6$ electrolyte lead to the formation of a SEI film, which has an unavoidable detrimental impact on the electrode performance as well as other side reactions with trace water or solvent-decomposed byproducts (Li_2CO_3, Li_2O, $ROCO_2Li$) on the surface of the electrode. The main surface reactions of $LiPF_6$ in EC/DMC solvents for the inorganic SEI formation on carbon electrodes are outlined in the following equations.[30,61,63]

$$PF_6^- + 3Li^+ + 2e^- \rightarrow 3LiF \downarrow + PF_3$$

$$LiPF_6 \leftrightarrow LiF + PF_5$$

$$PF_5 + H_2O \rightarrow 2HF + PF_3O$$

$$PF_5 + 2xLi^+ + 2xe^+ \rightarrow 2Li_xPF_{5-x} \downarrow + xLiF \downarrow$$

$$PF_3O + 2xLi^+ + 2xe^- \rightarrow Li_xPF_{3-x}O \downarrow + xLiF \downarrow$$

$$PF_5 + Li_2CO_3 \rightarrow 2LiF \downarrow + PF_3O + CO_2 \uparrow$$

$$LiPF_6 + Li_2CO_3 \rightarrow 3LiF \downarrow + PF_3O + CO_2 \uparrow$$

$$2HF + Li_2CO_3 \rightarrow 2LiF \downarrow + H_2O + CO_2 \uparrow$$

The major side reactions of solvent (EC/DMC) reduction products forming an organic SEI are given below.

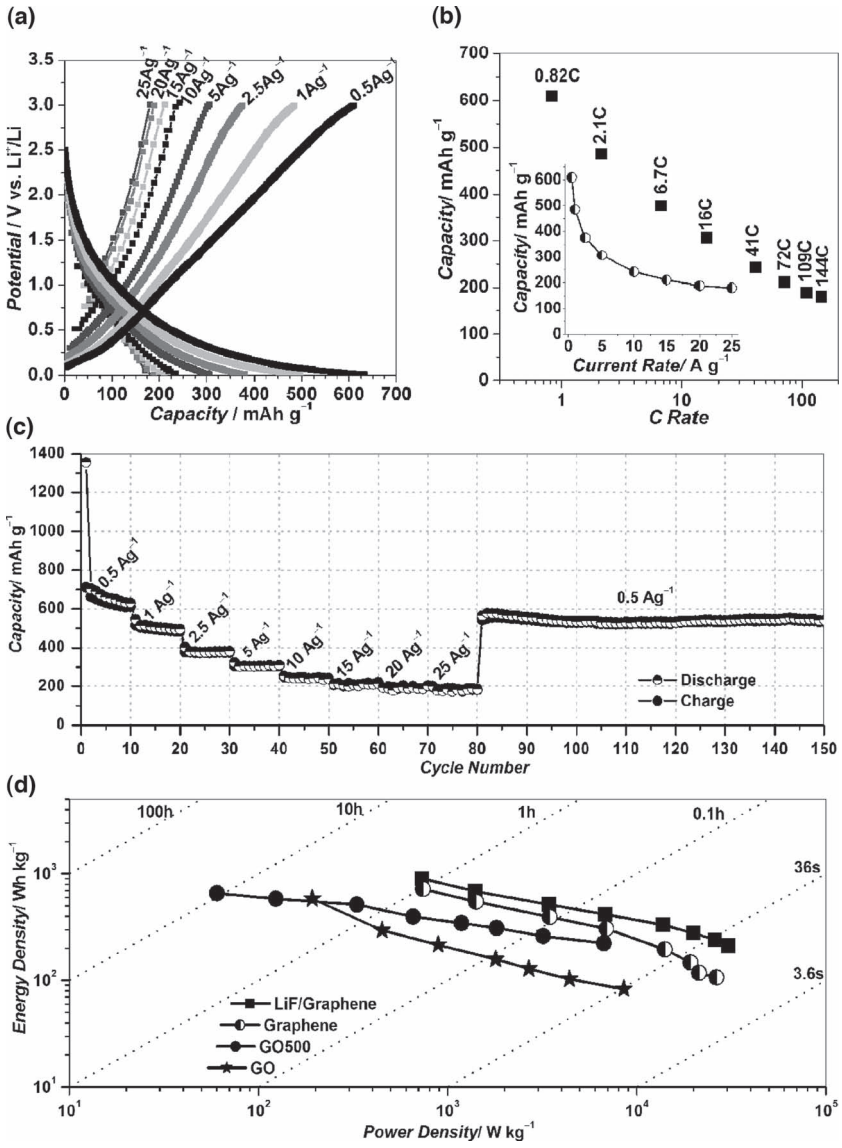

Figure 2. a) Galvanostatic charge-discharge profiles of the LiF/graphene electrode. b) Reversible capacity as a function of charging rates. *n*C denotes the rate at which a full charge takes 1/*n* hours. Inset: a plot of specific capacity vs. current rate. c) High-rate capability and cycling performance of the LiF/graphene electrode over a wide range of current densities from 0.5 A g^{-1} to 25 A g^{-1}. The profiles in (a) and the capacities in (b) correspond to the 10th cycle at each rate in (c). d) Ragone plot of the Li/LiF–modified graphene cell. For comparison, the electrochemical performance of graphene, GO, and GO treated at 500 °C (GO 500)[32] are also shown.

$$EC(CH_2O)_2\,CO + 2Li^+ + 2e^- \rightarrow Li_2CO_3 \downarrow + C_2H_4 \uparrow$$

$$EC\ 2\,(CH_2O)_2\,CO + 2Li^+ + 2e^- \rightarrow (CH_2OCO_2Li)_2 \downarrow + C_2H_4 \uparrow$$

$$DMC \quad CH_3OCO_2CH_3 + 2Li^+ + 2e^- \rightarrow Li_2CO_3 \downarrow + C_2H_6 \uparrow$$

$$DMC \quad 2CH_3OCO_2CH_3 + 2Li^+ + 2e^- \rightarrow 2CH_3OCO_2Li \downarrow + C_2H_6 \uparrow$$

As shown in the above equations, the corrosive reactions of electrolyte decomposition cannot be totally prevented, however, it should be possible to minimize them by controlled surface modification of the electrode and by the selective addition of electrolyte additives,[37,38] which allow the optimization of the SEI film formation.[35,64] As a result, the optimized SEI film will affect the passivation mechanism of the electrode towards the electrolyte[35] and improve the electrochemical reactivity of the electrode.[32,49]

To fully understand the influence of surface chemical properties of graphene on the electrode surface structure and performance during charge and discharge, we carried out SEM and XPS measurements on the SEI film formed on the pristine graphene and LiF/graphene electrodes. Before cycling, both of electrodes show very similar surface structures with graphene sheets and small irregularly-shaped carbon black agglomerates on their surface (**Figure 3**a,d), but many LiF nanoparticles can be clearly observed on the modified electrode. However, after cycling, they exhibit an apparent difference in surface structures. The graphene electrode surface shows an inhomogenous structure of the SEI film comprising protuberant particulate-type compounds (Figure 3b,c), which are inorganic Li salts, e.g., LiF, Li_2CO_3 and the polymeric species of the SEI film. Large cracks with a width up to micrometers in the SEI film are observed, which are caused by the electrode fading upon cycling. In sharp contrast, the LiF/graphene has a large-area continuous SEI film with a opened porous structure, and has a lower visible exposed graphene surface than the graphene electrode (Figure 3e,f), as revealed by EDX mapping (Figure S4,S5, Supporting Information). It was reported that the quality of a passivated SEI film on the carbon electrode has a significant influence on the Li storage performance of LIBs.[30,31] In the case of a pristine graphene electrode, a new SEI film is generated on the cracked areas upon cycling, resulting in the repeated consumption of lithium and the associated reduction of charge, and an increase in the average thickness of the SEI film. As a consequence, the increased SEI film thickness inhibits electrolyte penetration into the electrode pores or even blocks the pores, thus lowering the migration and diffusion rates of lithium ions in the electrode and decreasing its usable charge capacity.[30,31] On the other hand, the continuous porous SEI film formed in a LiF/graphene electrode is more favorable for both electrode stability and Li-ion transport, as demonstrated in Figure 2.

Figure 4 shows the XPS spectra of the surface and internal regions of the graphene and LiF/graphene electrodes. The internal region was exposed and measured by sputtering the electrode surface for 300 s, using Ar ion-beam. Table S1 (Supporting Information) summaries the assignments of all the deconvolved XPS peaks.[34,63,65,66] By comparing the XPS spectra of the graphene and LiF/graphene electrodes before

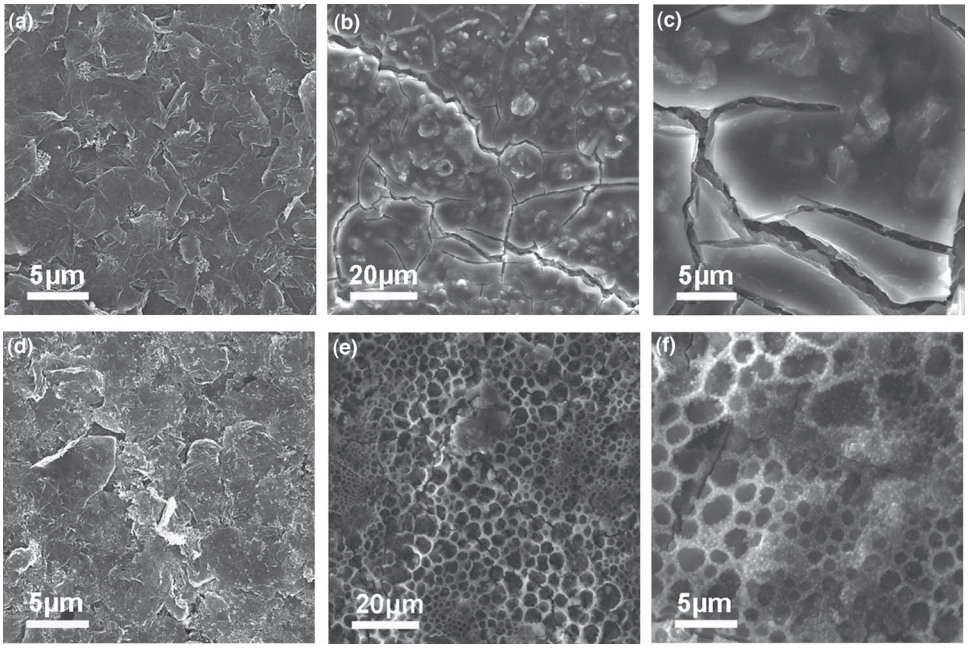

Figure 3. a–c) SEM images of the pristine graphene electrode surface (a) before and (b,c) after 10 cycles at 0.5 A g^{-1}. d–f) SEM images of the LiF/graphene electrode surface (d) before and (e,f) after 10 cycles at 0.5 A g^{-1}.

and after sputtering, a few important points are obtained: 1) In the C1s XPS spectra, the graphene electrode shows a much more pronounced shoulder peak of carbonates (i.e., Li_2CO_3 at 290.5 eV, $ROCO_2Li$ at 287–290 eV) than the LiF/graphene electrode.[34] After 300 s sputtering, these carbonate peaks nearly disappear for the modified graphene, while they are still clearly observed for the graphene electrode, though smaller than for the pristine sample. 2) In the O1s spectra, a small peak of Li_2O (529.0 eV) was observed from the SEI film on the graphene, but absent on the LiF/graphene after sputtering.[34,66] It is suggested that the presence of LiF could substantially decrease the amount of lithium- and alkyl- carbonates, and to some extent inhibit the solvent reduction. 3) Comparison of F1s and Li1s spectra, combined with the C1s and O1s spectra, shows that LiF dominates the inorganic SEI film on the LiF/graphene, while Li_2CO_3 and LiF dominate the inorganic SEI film on the graphene. The amounts of F and Li are far more increased for the pristine graphene than for the LiF/graphene after sputtering, which indicates a stronger electrolyte decomposition of $LiPF_6$ in the pristine graphene electrode.

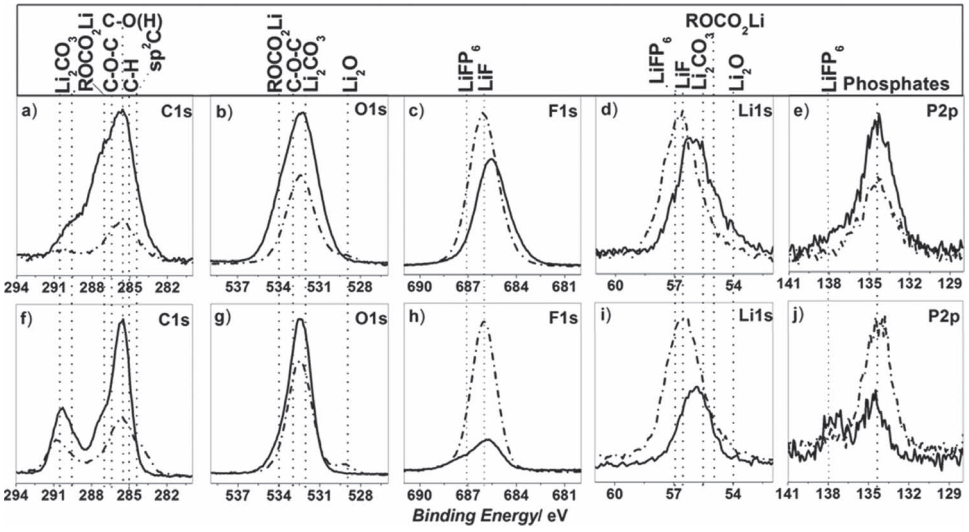

Figure 4. a) C1s, b) O1s, c) F1s, d) Li1s, e) P2p XPS spectra of the LiF/graphene electrode measured for 10 cycles at 0.5 A g^{-1} in $LiPF_6$+EC/DMC electrolyte at room temperature. f) C1s, g) O1s, h) F1s, i) Li1s, j) P2p XPS spectra of the pristine graphene electrodes measured for 10 cycles at 0.5 A g^{-1} in $LiPF_6$+EC/DMC electrolyte at room temperature. Black line: the pristine sample; dash dot line: the sample sputtered for 300 s. The C1s, O1s, F1s, Li1s, and P2p peaks were assigned to the corresponding components in a SEI layer (upper row).

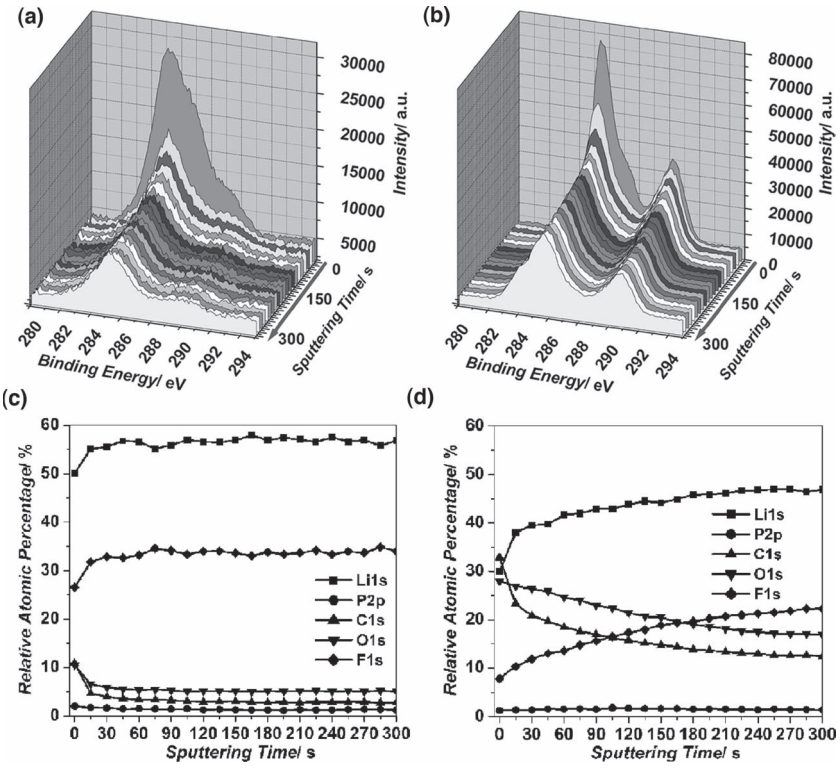

Figure 5. a,b) Depth profiles of C1s XPS spectra (a) the LiF/graphene and (b) the pristine graphene electrodes charged/discharged for 10 cycles at 0.5 A g^{-1}. c,d) Surface components of the SEI film as a function of Ar ion-beam sputtering time for (c) the LiF/graphene and (d) the pristine graphene electrodes charged/discharged for 10 cycles at 0.5 A g^{-1}.

4) The P2p spectrum generally consists of two major peaks of phosphate compounds (134.4 eV)[63] and $LiPF_6$ (138 eV).[63] On one hand, a $LiPF_6$-rich peak appears on the pristine graphene before sputtering but not on the modified graphene. On the other hand, the amount of phosphate in the SEI film increases for the graphene after sputtering, but decreases for the LiF/graphene electrode. All these results strongly suggest that the $LiPF_6$-electrolyte decomposition is significantly suppressed in the LiF/graphene.

In order to confirm the above observations, we studied the XPS spectra of the graphene and LiF/graphene electrodes at different sputtering depths (**Figure 5**). In the LiF/graphene, after a short sputtering time (15 s), the C1s XPS spectra confirm that the thin layer of carbonates ($ROCO_2Li$) is removed, and the amounts of other carbon components (i.e., C-O-C, C-O, C-H) and O, Li, F, P elements remain constant as the sputtering time increases (Figure 5a,c). For the pristine graphene, however, the carbonate peaks are still present in the C1s spectra, and slightly disappear with increasing sputtering time (Figure 5b,d). The Li and F signals increase with increasing sputtering time, indicating that the amount of LiF originating from the $LiFP_6$-electrolyte decomposition gradually increases from the surface of the SEI to the surface of the graphene. Meanwhile, the O signal decreases, revealing that the amount of carbonates resulting from the solvent-(EC/DMC) reduction gradually decreases (Figure 5c,d). It is worth noting that the LiF/graphene electrode shows high atomic percentages of Li and F but low percentages of C and O, further demonstrating that the SEI film is mainly composed of LiF. In the case of pristine graphene, the SEI film is composed of LiF and carbonates. This result suggests that a smaller amount of LiF covered on graphene can serve as a $LiPF_6$ salt stabilizer to effectively inhibit electrolyte decomposition and solvent reduction, and thus as an efficient SEI forming inhibitor to affect the inorganic/organic components and reduce the thickness of the passivated SEI film, as shown in Scheme 1.

All the above results suggest that the presence of LiF nanoparticles on graphene not only kinetically protects the $LiFP_6$ electrolyte from further decomposition, but also suppresses the reduction of the solvents, which is beneficial to the stability of the electrolytes, decreasing the production of heat and favoring the formation of a thin passivated SEI film with a porous structure. The resultant porous SEI film not only protects further electrolyte decomposition but also increases Li ion transport at the interface between electrode and electrolyte. The LiF on the graphene also provides an extra Li source for reducing the first-cycle irreversible capacity and producing nanochannels/micropores to increase the number of host sites for lithium storage. Meanwhile, the fluorinated compound (LiF) on the electrode surface helps improve interfacial compatibility between electrode and $LiFP_6$ electrolyte. Because of the above advantages of LiF surface modification together with the merits of graphene, such as a superior conducting network, a developed pore structure and good flexibility, the electrochemical performance of the LiF/graphene electrode, including rate capability and cycling stability, is markedly improved during fast charging and discharging.

3. Conclusions

A reliable surface modification strategy has been demonstrated to synthesize LiF nanoparticle-modified graphene as a high-power and high-energy LIB electrode material. The discrete crystalline LiF nanoparticles on the graphene surface effectively suppress electrolyte side reactions, affect the formation of both inorganic and organic SEI components, and consequently reduce the thickness of the SEI film formed, enabling fast Li ion transport at the interface between electrode and electrolyte. As a result, the LiF/graphene electrode shows a greatly improved electrochemical performance with large capacity, increased cycle life, and in particular, very high rate capability within tens of seconds. High accessible power and energy densities can be simultaneously achieved. This work provides new insights into

research and development of improved electrode solutions for high-power LIBs.

4. Experimental Section

Synthesis of LiF Nanoparticle-Modified Graphene: The graphene sheets used were synthesized by chemical exfoliation of flake graphite powder (500 mesh) and thermal reduction at 450 °C in a mixed gas of H_2 and Ar (1:4, v:v) with a flow rate of 50 mL min^{-1} in a Lindberg tube furnace as previously reported.[26] LiF-modified graphene was prepared in the following manner. Typically, graphene sheets (40 mg) were first dispersed in 40 mL ethanol for 15 min by sonication. Then 5 mL of $LiNO_3$ (5.7 mg) in ethanol was added to the suspension and vigorously stirred for 0.5 h at room temperature. Subsequently, 5 mL of NH_4F (10.65 mg) in ethanol was slowly added, and the mixed solution was continuously stirred for 2 h. The sample was then filtered and washed with ethanol several times, and finally dried at 60 °C in vacuum for 2 h, and annealed at 400 °C for 5 h in Ar gas in a Lindberg tube furnace.

Materials Characterizations: XPS measurements were conducted using an ESCALAB 250 with Al Kα (1486.6 eV) radiation under 1×10^{-9} Torr. To identify and determine the concentration of the elements on the electrode surface, coin-type cells after being used for 10 cycles at 0.5 A g^{-1} were disassembled in an argon-filled glove-box, and the graphene electrodes were retrieved, rinsed with diethyl carbonate, and dried under vacuum at room temperature for further XPS analysis. Depth profiling was performed by Ar ion-beam sputtering at ~2 keV (2 μA), and data was collected every 15 s for 5 min. The sputtering rate was estimated to be ~0.2 nm/s and changes in elemental composition were recorded as a function of sputtering time. Calibration of the peak position of surface elements was based on the graphitic peak in the C 1s spectrum at 284.5 eV. When the graphitic peak was not present or observable in the spectra, some reference compounds present on the electrode surface (i.e., LiF, Li_2CO_3, $LiPF_6$, and polyethylene oxide) were used. Respective binding energies were determined for surface elements of SEI films, and used to analyze the spectra of the electrode surface. SEM images and elemental mapping characterizations were performed using a FEI Nova Nano 430 system equipped with an EDX detector. TEM and HRTEM images were obtained using a Tecnai F30 TEM with an accelerating voltage of 300 kV. XRD measurements were conducted on D-MAX/2400 with a Rigaku Multiflex powder diffractometer with Cu Kα radiation between 5° and 80° and an incident wavelength of 0.154056 nm.

Electrochemical Measurements: Working electrodes were prepared by mixing 70 wt% graphene or Li-modified graphene, 15 wt% acetylene black (Super-P), and 15 wt% polyvinylidene fluoride (PVDF) binder dissolved in N-methyl-2-pyrrolidinone. After stirring and coating the slurries on Cu foils, the electrodes were dried at 120 °C in vacuum for 2 h to remove the solvent before pressing and cutting. Then the electrodes were dried at 100 °C for 24 h in vacuum. Cells (CR2032 type) were assembled in an argon-filled glove-box, using lithium metal as the counter/reference electrode, a Celgard 2400 membrane separator and 1 M $LiPF_6$ electrolyte solution dissolved in a mixture of ethylene carbonate (EC) and dimethyl carbonate (DMC, 1:1). Galvanostatic charge-discharge measurements were tested using a LAND CT2001A electrochemical workstation at different current densities of 0.5 ~ 25 A g^{-1} between 3 V and 0.01 V vs. Li^+/Li at room temperature.

The energy density (E) and power density (P) in a constant current charge-discharge process were calculated using the following equation:[32]

$$E = \int_0^t \frac{IV}{m} dt; \quad P = \frac{1}{t} \int_0^t \frac{IV}{m} dt$$

where I, V, m, and t are the current, voltage, mass of active material, and charge time, respectively, in a Li/graphene or Li/LiF-modified graphene cell. That is, the energy density (E) is the integrated area of the charge curve of voltage (V) vs. capacity (mAh g^{-1}, or Ah kg^{-1}), and the power density (P) is the energy density (E) divided by charge time (t) corresponding to the charge curve.

Supporting Information

Supporting Information is available from the Wiley Online Library or from the author.

Acknowledgements

This work was supported by National Science Foundation of China (No. 50921004, 50872136, and 50972147). The authors also thank X.H. Shao for TEM assistance.

Received: February 23, 2012
Published online: April 24, 2012

[1] J. M. Tarascon, M. Armand, *Nature* **2001**, *414*, 359.
[2] K. S. Kang, Y. S. Meng, J. Breger, C. P. Grey, G. Ceder, *Science* **2006**, *311*, 977.
[3] B. Kang, G. Ceder, *Nature* **2009**, *458*, 190.
[4] H. Li, Z. X. Wang, L. Q. Chen, X. J. Huang, *Adv. Mater.* **2009**, *21*, 4593.
[5] C. Liu, F. Li, L. P. Ma, H. M. Cheng, *Adv. Mater.* **2010**, *22*, E28.
[6] M. Winter, J. O. Besenhard, M. E. Spahr, P. Novak, *Adv. Mater.* **1998**, *10*, 725.
[7] M. S. Whittingham, *Chem. Rev.* **2004**, *104*, 4271.
[8] W. L. Lee, N. Yabuuchi, B. M. Gallant, S. Chen, B. S. Kim, P. T. Hammod, Y. Shao-Horn, *Nat. Nanotechnol.* **2010**, *5*, 531.
[9] V. Etacheri, R. Marom, R. Elazari, G. Salitra, D. Aurbach, *Energy Environ. Sci.* **2011**, *4*, 3243.
[10] S. M. Paek, E. Yoo, I. Honma, *Nano Lett.* **2009**, *9*, 72.
[11] D. H. Wang, D. W. Choi, J. Li, Z. G. Yang, Z. M. Nie, R. Kou, D. H. Hu, C. M. Wang, L. V. Saraf, J. G. Zhang, I. A. Aksay, J. Liu, *ACS Nano* **2009**, *3*, 907.
[12] Z. S. Wu, W. Ren, L. Wen, L. Gao, J. Zhao, Z. Chen, G. Zhou, F. Li, H. M. Cheng, *ACS Nano* **2010**, *4*, 3187.
[13] G. M. Zhou, D. W. Wang, F. Li, L. L. Zhang, N. Li, Z. S. Wu, L. Wen, G. Q. Lu, H. M. Cheng, *Chem. Mater.* **2010**, *22*, 5306.
[14] A. L. M. Reddy, A. Srivastava, S. R. Gowda, H. Gullapalli, M. Dubey, P. M. Ajayan, *ACS Nano* **2010**, *4*, 6337.
[15] Z. S. Wu, D. W. Wang, W. Ren, J. Zhao, G. Zhou, F. Li, H. M. Cheng, *Adv. Funct. Mater.* **2010**, *20*, 3595.
[16] Z. S. Wu, G. M. Zhou, L. C. Yin, W. C. Ren, F. Li, H. M. Cheng, *Nano Energy* **2012**, *1*, 107.
[17] H. L. Wang, L. F. Cui, Y. A. Yang, H. S. Casalongue, J. T. Robinson, Y. Y. Liang, Y. Cui, H. J. Dai, *J. Am. Chem. Soc.* **2010**, *132*, 13978.
[18] X. Zhu, Y. Zhu, S. Murali, M. D. Stoller, R. S. Ruoff, *ACS Nano* **2011**, *5*, 3333.
[19] S. B. Yang, X. L. Feng, S. Ivanovici, K. Müllen, *Angew. Chem. Int. Ed.* **2010**, *49*, 8408.
[20] S. B. Yang, X. L. Feng, L. Wang, K. Tang, J. Maier, K. Müllen, *Angew. Chem. Int. Ed.* **2010**, *49*, 4795.
[21] S. B. Yang, X. L. Feng, K. Müllen, *Adv. Mater.* **2011**, *23*, 3575.
[22] J. Xiao, X. J. Wang, X. Q. Yang, S. D. Xun, G. Liu, P. K. Koech, J. Liu, J. P. Lemmon, *Adv. Funct. Mater.* **2011**, *21*, 2840.
[23] N. Li, G. Liu, C. Zhen, F. Li, L. L. Zhang, H. M. Cheng, *Adv. Funct. Mater.* **2011**, *21*, 1717.
[24] Z. J. Fan, J. Yan, T. Wei, L. J. Zhi, G. Q. Ning, T. Y. Li, F. Wei, *Adv. Funct. Mater.* **2011**, *21*, 2366.

[25] S. Park, R. S. Ruoff, *Nat. Nanotechnol.* **2009**, *4*, 217.
[26] Z. S. Wu, W. Ren, L. Gao, B. Liu, C. Jiang, H. M. Cheng, *Carbon* **2009**, *47*, 493.
[27] Z. S. Wu, W. C. Ren, L. B. Gao, J. P. Zhao, Z. P. Chen, B. L. Liu, D. M. Tang, B. Yu, C. B. Jiang, H. M. Cheng, *ACS Nano* **2009**, *3*, 411.
[28] Y. Liang, D. Wu, X. Feng, K. Müllen, *Adv. Mater.* **2009**, *21*, 1679.
[29] D. R. Dreyer, S. Park, C. W. Bielawski, R. S. Ruoff, *Chem. Soc. Rev.* **2010**, *39*, 228.
[30] W. Schalkwijk, B. Scrosati, *Advances in Lithium Ion Batteries*, Kluwer Academic/Plenem Publisher, New York, USA **2002**.
[31] M. Winter, *Z. Phys. Chem.* **2009**, *223*, 1395.
[32] Z. S. Wu, W. Ren, L. Xu, F. Li, H. M. Cheng, *ACS Nano* **2011**, *5*, 5463.
[33] E. Peled, D. Golodnitsky, G. Ardel, *J. Electrochem. Soc.* **1997**, *144*, L208.
[34] P. Verma, P. Maire, P. Novak, *Electrochim. Acta* **2010**, *55*, 6332.
[35] L. J. Fu, H. Liu, C. Li, Y. P. Wu, E. Rahm, R. Holze, H. Q. Wu, *Solid State Sci.* **2006**, *8*, 113.
[36] G. Nadeau, X. Y. Song, M. Masse, A. Guerfi, G. Brisard, K. Kinoshita, K. Zaghib, *J. Power Sources* **2002**, *108*, 86.
[37] S. S. Zhang, *J. Power Sources* **2006**, *162*, 1379.
[38] D. Aurbach, Y. Talyosef, B. Markovsky, E. Markevich, E. Zinigrad, L. Asraf, J. S. Gnanaraj, H. J. Kim, *Electrochim. Acta* **2004**, *50*, 247.
[39] F. Coowar, A. M. Christie, P. G. Bruce, C. A. Vincent, *J. Power Sources* **1998**, *75*, 144.
[40] G. H. Wrodnigg, T. M. Wrodnigg, J. O. Besenhard, M. Winter, *Electrochem. Commun.* **1999**, *1*, 148.
[41] W. H. Yao, Z. R. Zhang, J. Gao, J. Li, J. Xu, Z. C. Wang, Y. Yang, *Energy Environ. Sci.* **2009**, *2*, 1102.
[42] H. Ota, A. Kominato, W. J. Chun, E. Yasukawa, S. Kasuya, *J. Power Sources* **2003**, *119*, 393.
[43] H. H. Lee, Y. Y. Wang, C. C. Wan, M. H. Yang, H. C. Wu, D. T. Shieh, *J. Appl. Electrochem.* **2005**, *35*, 615.
[44] Y. X. Wang, S. Nakamura, K. Tasaki, P. B. Balbuena, *J. Am. Chem. Soc.* **2002**, *124*, 4408.
[45] X. Sun, H. S. Lee, X. Q. Yang, J. McBreen, *Electrochem. Solid State Lett.* **2002**, *5*, A248.
[46] Y. S. Hu, W. H. Kong, Z. X. Wang, X. J. Huang, L. Q. Chen, *Solid State Ionics* **2005**, *176*, 53.
[47] Y. EinEli, S. R. Thomas, V. R. Koch, *J. Electrochem. Soc.* **1997**, *144*, 1159.
[48] D. Aurbach, Y. Eineli, O. Chusid, Y. Carmeli, M. Babai, H. Yamin, *J. Electrochem. Soc.* **1994**, *141*, 603.
[49] F. Beguin, E. Frackowiak, *Carbons for Electrochemical Energy Storage and Conversion Systems*, CRC Press, Taylor & Francis Group, Boca Raton, FL **2010**.
[50] J. Vetter, P. Novak, M. R. Wagner, C. Veit, K. C. Moller, J. O. Besenhard, M. Winter, M. Wohlfahrt-Mehrens, C. Vogler, A. Hammouche, *J. Power Sources* **2005**, *147*, 269.
[51] H. L. Wang, J. T. Robinson, G. Diankov, H. J. Dai, *J. Am. Chem. Soc.* **2010**, *132*, 3270.
[52] P. V. Kamat, *J. Phys. Chem. Lett.* **2010**, *1*, 520.
[53] H. Buqa, D. Goers, M. Holzapfel, M. E. Spahr, P. Novak, *J. Electrochem. Soc.* **2005**, *152*, A474.
[54] Y. S. Hu, P. Adelhelm, B. M. Smarsly, S. Hore, M. Antonietti, J. Maier, *Adv. Funct. Mater.* **2007**, *17*, 1873.
[55] Y. J. Xu, X. Liu, G. L. Cui, B. Zhu, G. Weinberg, R. Schlogl, J. Maier, D. S. Su, *ChemSusChem* **2010**, *3*, 343.
[56] H. Y. Wang, T. Abe, S. Maruyama, Y. Iriyama, Z. Ogumi, K. Yoshikawa, *Adv. Mater.* **2005**, *17*, 2857.
[57] V. Subramanian, H. W. Zhu, B. Q. Wei, *J. Phys. Chem. B* **2006**, *110*, 7178.
[58] D. N. Futaba, K. Hata, T. Yamada, T. Hiraoka, Y. Hayamizu, Y. Kakudate, O. Tanaike, H. Hatori, M. Yumura, S. Iijima, *Nat. Mater.* **2006**, *5*, 987.
[59] S. Y. Chung, J. T. Bloking, Y. M. Chiang, *Nat. Mater.* **2002**, *1*, 123.
[60] Y. J. Lee, H. Yi, W. J. Kim, K. Kang, D. S. Yun, M. S. Strano, G. Ceder, A. M. Belcher, *Science* **2009**, *324*, 1051.
[61] D. Aurbach, *J. Power Sources* **2000**, *89*, 206.
[62] S. Leroy, H. Martinez, R. Dedryvere, D. Lemordant, D. Gonbeau, *Appl. Surf. Sci.* **2007**, *253*, 4895.
[63] S. Leroy, F. Blanchard, R. Dedryvere, H. Martinez, B. Carre, D. Lemordant, D. Gonbeau, *Surf. Interface Anal.* **2005**, *37*, 773.
[64] M. Wachtler, M. Winter, J. O. Besenhard, *J. Power Sources* **2002**, *105*, 151.
[65] A. M. Andersson, K. Edstrom, *J. Electrochem. Soc.* **2001**, *148*, A1100.
[66] V. Eshkenazi, E. Peled, L. Burstein, D. Golodnitsky, *Solid State Ionics* **2004**, *170*, 83.